A genome-wide MAGIC kit for recombinase-independent mosaic analysis in *Drosophila*

Yifan Shen[1], Ann T. Yeung[1,2], Payton Ditchfield[3], Elizabeth Korn, Rhiannon Clements, Xinchen Chen[4], Bei Wang, Zixian Huang[5] Michael Sheen[6], Parker A. Jarman[7], and Chun Han*

Department of Molecular Biology and Genetics, Cornell University, Ithaca, New York, USA

Weill Institute for Cell and Molecular Biology, Cornell University, Ithaca, New York, USA

[1]These authors contributed equally.

[2]Current address: Harvard Medical School, Boston, MA 02115, USA

[3]Current address: Center for Community Independence, Revere, MA 02151, USA

[4]Current address: Department of Neurobiology, School of Biological Sciences, University of California, San Diego, La Jolla, CA 92093, USA.

[5]Current address: Department of Developmental Biology, Washington University School of Medicine, Saint Louis, MO 63110, USA

[6]Current address: Warren Alpert Medical School of Brown University, Providence, RI 02903, USA

[7]Current address: Yale School of Medicine, New Haven, CT 06510, USA

*For correspondence: chun.han@cornell.edu (CH)

ABSTRACT

Mosaic analysis has been instrumental in advancing developmental and cell biology. Most current mosaic techniques rely on exogenous site-specific recombination sequences that need to be introduced into the genome, limiting their application. Mosaic analysis by gRNA-induced crossing-over (MAGIC) was recently developed in *Drosophila* to eliminate this requirement by inducing somatic recombination through CRISPR/Cas9-generated DNA double-strand breaks. However, MAGIC has not been widely adopted because gRNA-markers, a required component for this technique, are not yet available for most chromosomes. Here, we present a complete, genome-wide gRNA-marker kit that incorporates optimized designs for enhanced clone induction and more effective clone labeling in both positive MAGIC (pMAGIC) and negative MAGIC (nMAGIC). With this kit, we demonstrate clonal analysis in a broad range of *Drosophila* tissues, including cell types that have been difficult to analyze using recombinase-based systems. Notably, MAGIC enables clonal analysis of pericentromeric genes and deficiency chromosomes and in interspecific hybrid animals, opening new avenues for gene function study, rapid gene discovery, and understanding cellular basis of speciation. This MAGIC kit complements existing systems and makes mosaic analysis accessible to address a wider range of biological questions.

IMPACT STATEMENT

A comprehensive toolkit enables genome-wide, recombinase-independent mosaic analysis in *Drosophila*, permitting clonal analysis of pericentromeric genes, deficiency chromosomes, and interspecific hybrids previously inaccessible to standard methods.

INTRODUCTION

Mosaic animals containing genetically distinct populations of cells in the same organism are useful for *in vivo* studies of complex biological processes. For this reason, techniques that can generate genetically labeled mosaic clones have been utilized in both vertebrates and invertebrates to study tissue-specific functions of pleiotropic genes, developmental timing, cell lineages, cell proliferation, neural wiring, and many other biological phenomena (Xu and Rubin 2012, Griffin, Binari et al. 2014, Germani, Bergantinos et al. 2018). The most popular mosaic techniques rely on site-specific recombination systems, such as FRT/Flp (Golic and Lindquist 1989, Xu and Rubin 1993) and LoxP/Cre (Zong, Espinosa et al. 2005, Henner, Ventura et al. 2013), to induce somatic recombination between homologous chromosomes. Such techniques require the introduction of recombination sites to specific locations in the genome and thus cannot be applied to unmodified chromosomes. To overcome this limitation, we recently developed a recombinase-independent mosaic technique called mosaic analysis by gRNA-induced crossing-over (MAGIC) (Allen, Koreman et al. 2021). In MAGIC, the CRISPR/Cas9 system generates double-strand breaks (DSBs) at a predefined genome location to induce homologous recombination in precursor cells during S/G2 phase. Subsequent chromosomal segregation during mitosis can result in clones homozygous for the chromosomal segments distal to the crossover site (Figure 1 - figure supplement 1A). Two variants of this technique in *Drosophila*, positive MAGIC (pMAGIC) and negative MAGIC (nMAGIC), label the resulting homozygous clones by the presence and absence of fluorescent markers, respectively (Figure 1 - figure supplement 1B) (Allen, Koreman et al. 2021). Like FRT/Flp-based techniques, MAGIC enables characterization of homozygous clones of lethal mutations in otherwise heterozygous animals (Allen, Koreman et al. 2021) (e.g. Figure 1 - figure supplement 1C).

However, unlike FRT/Flp-based techniques, MAGIC does not require prior genetic modification of the test chromosome. Thus, it can potentially be used on any chromosome and have much wider applications. Foremost, mutations of diverse natures have been established for most *Drosophila* genes (Hacker, Nystedt et al. 2003, Bellen, Levis et al. 2004, Thibault, Singer et al. 2004, Staudt, Molitor et al. 2005, Bellen, Levis et al. 2011, Yamamoto, Jaiswal et al. 2014), and thousands of deficiency strains harbor deletions that collectively uncover 98.4% of the *Drosophila* genome (Cook, Christensen et al. 2012). However, most of these mutant chromosomes cannot be analyzed by traditional mosaic techniques due to the lack of FRT sites

70 or incompatibility with the FRT/Flp system. Although FRT sites can be introduced onto mutant
71 chromosomes through genetic recombination, this process is labor-intensive and time-consuming
72 and thus is impractical at a large scale. In contrast, MAGIC can theoretically be applied to any
73 existing stock, including those from classical mutagenesis screens and deficiency libraries,
74 allowing convenient genome-wide mosaic screens. In addition, genes located more proximal to
75 centromeres than existing FRT sites cannot be analyzed by FRT/Flp techniques. In comparison,
76 MAGIC can potentially be used to study these genes because the crossover site in MAGIC can
77 be flexibly defined by users. Lastly, given that MAGIC is compatible with wild-derived
78 chromosomes (Allen, Koreman et al. 2021), it may be able to generate homozygous clones of a
79 chromosome derived from a single species in an interspecific hybrid animal, allowing the study
80 of species-related cell-cell interactions.

81 Despite these potentials, MAGIC has not been widely adopted by the *Drosophila*
82 community. A major barrier is the lack of gRNA-marker transgenes on most chromosomal arms,
83 which are necessary for DSB induction and fluorescent clone labeling (Allen, Koreman et al.
84 2021). In addition, the existing gRNA-markers suffer from several limitations, including low
85 frequency of clone induction, weak labeling of pMAGIC clones, and suboptimal visualization of
86 nMAGIC clones. Because of these reasons, MAGIC has only been successfully applied to a few
87 genes in a limited number of *Drosophila* tissues (Allen, Koreman et al. 2021, Chen, Wang et al.
88 2025).

89 To overcome these limitations, here we first optimized gRNA-marker designs to improve
90 clonal induction, the brightness of pMAGIC clones, and visualization of nMAGIC clones. Then
91 we generated pMAGIC and nMAGIC gRNA-markers for all chromosomal arms and
92 characterized their ability to generate clones. Using this kit, we demonstrate mosaic analysis of
93 centromere-proximal genes, deficiency chromosomes, chromosomes derived from different
94 *Drosophila* species in interspecific hybrid animals. This kit allows optimal clone induction in
95 diverse cell and tissue types and should be useful for studying a wide range of biological
96 processes.

97 **RESULTS**

98 **New gRNA-marker designs improve pMAGIC and nMAGIC**

99 MAGIC relies on a gRNA-marker dual-transgene (Figure 1A and Figure 1 - figure supplement
100 1B) inserted in a specific chromosomal arm to both induce and visualize clones homozygous for
101 this arm (Allen, Koreman et al. 2021). The gRNA part of the construct expresses two gRNAs
102 ubiquitously to target a pericentromeric location on this arm. Two gRNAs targeting two
103 sequences that are close to each other, instead of a single gRNA, are used to increase the
104 probability of DSBs and thus the clone frequency. The marker part in pMAGIC utilizes a
105 ubiquitously expressed Gal80 to prevent Gal4-dependent labeling of heterozygous and
106 homozygous cells for the gRNA-marker, while allowing labeling of homozygous cells that lose
107 the gRNA-marker. In contrast, nMAGIC uses ubiquitously expressed BFP, which results in
108 brighter labeling of gRNA-marker homozygous cells, intermediate labeling of gRNA-marker
109 heterozygous cells, and lack of labeling of gRNA-marker-negative homozygous cells (Figure 1 -
110 figure supplement 1B).

111 We have previously developed gRNA-marker vectors for both pMAGIC and nMAGIC.
112 However, gRNA-markers made with these vectors exhibit some limitations. First, the clone
113 frequency can be low for certain gRNAs (Allen, Koreman et al. 2021). Second, the *ubi-Gal80* in
114 pMAGIC gRNA-markers does not completely suppress Gal4 activity in certain tissues, such as
115 hemocytes. Third, pMAGIC clones are sometimes too dim to visualize cell morphology, such as
116 thin dendrite and axon projections of neurons. Lastly, nMAGIC utilizes a nuclear BFP marker
117 (nlsBFP), which does not show the cell shape and sometimes cannot mark clones effectively.
118 Thus, to optimize MAGIC, we first sought to improve the gRNA-marker designs.

119 Since clone induction in MAGIC depends on gRNA-induced DNA DSBs, we asked
120 whether a more efficient gRNA design enhances clone frequency in somatic tissues. The
121 previous gRNA-marker vectors used a tgFE design, which contains a flip of A-U positions and a
122 stem-loop extension (F+E) of the original gRNA scaffold and a $tRNA^{Gly}$ before each gRNA
123 targeting sequence (Figure 1A) (Allen, Koreman et al. 2021). However, we have shown that an
124 improved Qtg2.1 design, which contains an additional extension of the second stem loop in the
125 gRNA scaffold (gRNA2.1) and a single $tRNA^{Gln}$ spacer between the two gRNAs (Figure 1A), is
126 much more mutagenic than tgFE in somatic tissues (Koreman, Xu et al. 2021). We thus
127 compared two pMAGIC gRNA-markers that are based on these two gRNA designs but target the
128 same genomic sequences at cytological band 40D2 to assess their ability to induce clones in
129 peripheral sensory neurons. When used with the same neuronal/epidermal precursor Cas9, *zk-*

130 *Cas9* (Allen, Koreman et al. 2021), Qtg2.1 resulted in three times more neuronal clones as
131 compared to tgFE (Figure 1B), confirming a positive correlation between gRNA efficiency and
132 clone frequency.

133 To ensure more complete suppression of Gal4 activity by Gal80 in pMAGIC, we
134 replaced the *ubi* enhancer driving Gal80 expression with an *αTub84B* (*tub*) enhancer that was
135 used in *tub-Gal80* in the MARCM system (Lee and Luo 1999). When combined with the larval
136 hemocyte marker *pxn-Gal4 UAS-CD4-tdTom* (Han, Song et al. 2014) (Figure 1C), *ubi-Gal80* did
137 not completely suppress the labeling of hemocytes (Figure 1D). In contrast, no labeled
138 hemocytes could be detected in the presence of *tub-Gal80* (Figure 1E), suggesting that *tub-Gal80*
139 is a better marker for pMAGIC.

140 To improve clone brightness in pMAGIC, we sought to destabilize Gal80 and reduce its
141 expression, reasoning that dim clones are due to prolonged Gal80 activity after clone induction.
142 In addition to replacing the *ubi* enhancer with the *tub* enhancer, we also introduced protein and
143 mRNA destabilization sequences (DE) (Zubiaga, Belasco et al. 1995, Li, Zhao et al. 1998) at the
144 3' end of the Gal80 coding sequence, and replaced the *His2Av* polyA by *SV40* polyA (Figure
145 1F), as the latter reduces transgene expression (Han, Jan et al. 2011). By measuring the
146 brightness of epidermal (Figure 1G) and neuronal (Figure 1H) clones induced by *gRNA-40D2*
147 and *gRNA-42A4*, we found that each of the three changes improved clone brightness.

148 Finally, to visualize cell shape in nMAGIC, we replaced nlsBFP with cytosolic BFP
149 tagged by 3X Hemagglutinin (HA), in addition to utilizing the *tub* enhancer. This new design
150 allowed us to better discern clone shapes in both the wing imaginal disc and the epidermis
151 (Figure 1J, 1J', and 1L), in contrast to the previous *ubi-nlsBFP* design (Figure 1I and 1K). To
152 make nMAGIC compatible with more fluorescent reagents, we generated an additional vector
153 that contains miRFP680, a far-red/infrared fluorescent protein (IFP) (Matlashov, Shcherbakova
154 et al. 2020), in place of BFP. Wing-disc clones labeled with this marker were readily detectable
155 in unstained tissues (Figure 1M). By measuring the sizes of homozygous gRNA-marker clones
156 (*BFP*/*BFP*) and homozygous wildtype (WT) clones (+/+) in wing discs, we found that these two
157 cell populations in the twin spots showed no noticeable bias in growth or viability (Figure 1O).

158 Thus, by altering the designs of the gRNAs and the Gal80 and BFP markers, we created
159 new vectors optimized for more robust applications of nMAGIC and pMAGIC.

160 **A gRNA-marker kit is established for all four chromosomes of *Drosophila***

161 To enhance the utility of MAGIC in *Drosophila*, we generated complete sets of pMAGIC and
162 nMAGIC (BFP version) gRNA-markers for all four chromosomes (Figure 2A). To identify
163 suitable gRNA target sites, we analyzed the pericentromeric sequences of X, 2L, 2R, 3L, 3R, and
164 4, based on three criteria (Allen, Koreman et al. 2021): conserved in closely related *Drosophila*
165 species to minimize the chance of single nucleotide polymorphism, (2) located away from
166 functionally critical regions to avoid disrupting essential processes, and (3) unique within the
167 genome to minimize off-target effects. For each MAGIC construct, we selected a pair of non-
168 repetitive gRNA target sequences in intergenic regions to maximize the chances of DSBs. These
169 two sequences are closely linked to minimize the risk of large deletions. Given the variable
170 efficiency of gRNA target sequences, we selected three pairs of gRNAs targeting three
171 chromosomal locations for each chromosomal arm and named them according to the
172 corresponding cytoband (Table 1).

173 To evaluate the clone-induction properties of these gRNAs, we combined the pMAGIC
174 set with *zk-Cas9* and counted the number of neuronal clones in A1-A7 larval hemi-segments
175 (Figure 2B). As expected, the clone frequency varied from gRNA to gRNA, but we were able to
176 identify efficient gRNAs (>= 10 clones per larva) for every chromosomal arm. We previously
177 found that different gRNAs follow the same trend of relative efficiency in different tissues
178 (Allen, Koreman et al. 2021). Here we additionally tested nMAGIC gRNAs for 2R in the wing
179 disc (Figure 2C) and noticed a similar trend of clone induction to that of their pMAGIC
180 counterparts in sensory neurons (Figure 2B), suggesting that the results in sensory neurons are
181 transferrable to other tissues.

182 Certain gRNAs (e.g. gRNA-40E1) exhibited very low clone frequency. Such gRNAs can
183 be useful for inducing sparse clones in highly packed tissues such as the brain. For example,
184 using the same *ey-Cas9* (Ji, Sapar et al. 2022), the highly efficient gRNA-40D2 induced too
185 many neuronal clones in the adult brain for morphological analysis (Figure 2D), while gRNA-
186 40E1 gave rise to few clones, whose projection patterns were much easier to analyze (Figure
187 2E).

188 Together, the pMAGIC and nMAGIC gRNA-marker lines constitute a complete kit
189 (Table 1) for genome-wide MAGIC applications in *Drosophila*.

190 **MAGIC allows clonal analysis in diverse tissues and cell types**

191 To determine if MAGIC can be applied to diverse tissues in *Drosophila*, we conducted clonal
192 analysis in the larva using *gRNA-40D2(Gal80)* and several tissue-specific Cas9s. With the
193 ubiquitous *vas-cas9* (Lopez Del Amo, Juste et al. 2022) and *tub-Gal4>UAS-mCD8-GFP*, we
194 readily detected clones in the larval brain (Figure 3A), proliferating tissues like eye and leg discs
195 (Figure 3B-C), and polyploid tissues like the fat body, gut, and trachea (Figure 3D-F). Clone
196 induction in polyploid tissues suggests that crossing-over events occurred before the last cell
197 division. Using *zk-cas9* and *R38F11-Gal4>UAS-tdTomato (tdTom)*, we observed frequent
198 epidermal clones (Figure 3G). Using the glia precursor *gcm-Cas9* and *repo-Gal4>UAS-mCD8-*
199 *GFP*, we detected individual glial clones in the brain (Figure 3H). The new pMAGIC gRNA-
200 marker design allowed us to reliably induce hemocyte clones (Figure 3I).

201 The ability to control the timing of clone induction has been instrumental for neuronal
202 birth dating and modulation of clone frequency in traditional MARCM analysis of the
203 *Drosophila* adult brain. To explore the potential of pMAGIC to serve similar purposes, we used
204 heat-shock (hs) Cas9 (Garcia-Marques, Espinosa-Medina et al. 2020), along with *gRNA-*
205 *40D(Gal80)* and a pan-neuronal Gal4/UAS-membrane marker combination (*RabX4-Gal4>UAS-*
206 *MApHS*), to induce neuronal clones in the adult brain. Heat shock at 120 h after egg laying
207 (AEL) induced too many clones for separating individual neurons (Figure 3J-J'), while later heat
208 shock at 48 h after pupal formation (APF) produced many fewer, spatially separated clones in the
209 central brain. These results collectively demonstrate MAGIC's efficacy and flexibility in
210 generating clones in diverse *Drosophila* tissues, indicating its value in studying gene function
211 and cell lineage in various tissue contexts.

212 The neuromuscular junction (NMJ) in *Drosophila* larvae has been a valuable model for
213 elucidating synaptic biology, owing to its simplicity, accessibility, and conserved features shared
214 with mammalian excitatory synapses (Menon, Carrillo et al. 2013, Charng, Yamamoto et al.
215 2014, Chou, Johnson et al. 2020). Despite its popularity, the NMJ has rarely been analyzed by
216 the MARCM technique in the literature, likely due to the difficulty of inducing clones in motor
217 neurons. To test the effectiveness of MAGIC in analyzing gene function at the NMJ, we selected
218 two genes crucial for synaptic function and construction: *Vesicular glutamate transporter*
219 (*VGlut*) (Daniels, Collins et al. 2004) and *bruchpilot* (*brp*) (Kittel, Wichmann et al. 2006, Wagh,

220 Rasse et al. 2006), null mutations of each of which exhibit recessive lethality in larvae.
221 Combined with appropriate gRNA(Gal80) lines (42A4 for *VGlut* on 2R and 40D2 for *brp* on 2L)
222 and *tub-Gal4 UAS-CD8-GFP*, *zk-Cas9* induced frequent clones in type Ib boutons (Figure 4A-
223 B"). The loss of VGlut or Brp specifically in GFP-labeled NMJs was confirmed by
224 immunostaining. These results exemplify the value of pMAGIC for dissecting gene function in
225 NMJ biology at the single cell level.

226 **MAGIC enables clonal analysis of pericentromeric genes, 4th chromosome-associated**
227 **mutations, and in interspecific hybrid animals**

228 Because all FRT sites in the existing FRT/Flp mosaic system are located at some distances away
229 from centromeres, it has not been possible to study genes located between the FRT sites and the
230 corresponding centromeres by clonal analysis. In contrast, the gRNA target site in a MAGIC
231 experiment can be user-selected to enable clonal analysis of any given gene. To illustrate this
232 potential, we used *gRNA-41F9* to induce homozygous mutant clones of *Ecdysone receptor*
233 (*EcR*), which is located at 42A10 and is inaccessible to all FRT sites on 2R. EcR is a
234 transcription factor required for neuronal remodeling during metamorphosis (Brown, Cherbas et
235 al. 2006). In peripheral sensory neurons, EcR activation at the beginning of pupariation causes
236 apoptosis of some dendritic arborization (da) neurons while triggering dendrite pruning of other
237 da neurons (Williams and Truman 2005). As expected, a wildtype (WT) pMAGIC clone of class
238 IV da (C4da) neuron exhibited complete dendrite pruning at 16 h after puparium formation
239 (APF), accompanied by dendrite debris phagocytosed into epidermal cells (Han, Song et al.
240 2014) (Figure 5A). In contrast, *EcR* mutant da neuron clones still maintained larval dendritic
241 arbors at 16 h APF (Figures 5B-D), instead of dying (in the case of C3da) or undergoing dendrite
242 pruning (in the cases of C1da and C4da).

243 Mosaic analysis of genes located on the 4th chromosome had not been possible until
244 recent introduction of FRT sites onto this chromosome by CRISPR-mediated knock-in
245 (Goldsmith, Shimell et al. 2022). Despite these advances, existing mutations on FRT-lacking 4th
246 chromosomes still cannot be analyzed by the FRT/Flp system, given that meiotic recombination
247 is exceedingly rare on the 4th chromosome, preventing introduction of FRT sites onto mutant
248 chromosomes. A valuable gene-disruption resource in *Drosophila* is the deficiency library
249 consisting of strains harboring chromosomal deletions. MAGIC can potentially be used in

250 conjunction with the deficiency library to screen for genes important in a particular biological
251 process. To test the potential of MAGIC for analyzing mutations on the 4th chromosome and for
252 gene discovery with deficiencies, we generated pMAGIC C4da clones of *Df(4)ED6380*, a
253 deficiency that deletes a segment between cytological bands 102B7 and 102D5. These clones
254 show dramatically reduced dendrites compared to the WT controls (Figure 5E-5G), indicating
255 the existence of genes important for dendrite growth in this region.

256 When examining nMAGIC gRNA-markers for the 4th chromosome, we noticed uneven
257 expression of *tub-3xHA-BFP* in epidermal cells and some imaginal tissues, exemplified by cells
258 lacking detectable BFP signal (Figure 5 – figure supplement 1A and B). This variegated
259 expression is likely due to transgenes residing in heterochromatin and is common for transgenes
260 located on the 4th chromosome (Riddle, Minoda et al. 2011). While this uneven expression limits
261 the usefulness of our gRNA-markers in the corresponding epithelial tissues, Gal80 in pMAGIC
262 gRNA-markers efficiently suppressed Gal4 activities in most neurons (Figure 5 – figure
263 supplement 1C), conforming their effectiveness in neuronal MAGIC analysis.

264 Lastly, we wondered if the MAGIC system can generate clones in interspecific hybrid
265 animals derived from *D. melanogaster* and *D. simulans* parents, given that the two species show
266 a large degree of synteny (Chakraborty, Chang et al. 2021). The clones in these animals would
267 contain homozygous chromosomal arms derived from a single species. To test this idea, we
268 crossed *D. melanogaster* females containing *gRNA-42A4(BFP); hh-cas9* to *D. simulans* males
269 carrying a loss of function mutation of *Lethal hybrid rescue mutation* (*Lhr*), which ensures the
270 viability of the hybrid male progeny (Barbash 2010). Indeed, we observed twin spots consisting
271 of dark clones, containing only *D. simulans* 2R, and brighter clones, containing only *D.*
272 *melanogaster* 2R, in wing discs of both female and male progeny (Figure 5G and 5H),
273 demonstrating the feasibility of studying species-specific alleles in cell-cell interactions in
274 interspecific hybrids.

275 **DISCUSSION**

276 Conceptually, MAGIC is a simpler and more convenient mosaic technique compared to
277 traditional recombinase-dependent methods. Theoretically, it can be applied directly to any
278 existing stock, including those that are not currently compatible with the FRT/Flp system.
279 However, the lack of gRNA-marker transgenes has prevented its wide application in *Drosophila*.

280 In this study, we present a complete gRNA-marker kit that enables genome-wide MAGIC in
281 *Drosophila*, removing this bottleneck. The new gRNA-markers incorporate optimized designs
282 that improve clone frequency and labeling in both pMAGIC and nMAGIC. We further
283 demonstrate the compatibility of MAGIC with broad tissues and cell types. More importantly,
284 MAGIC enables mosaic analyses that could not be accomplished by existing FRT/Flp systems,
285 such as those of pericentromeric genes, deficiency chromosomes, and interspecific homologous
286 chromosomes. Thus, this MAGIC kit provides *Drosophila* researchers with greater flexibility for
287 conducting mosaic analyses of diverse purposes.

288 To implement MAGIC, one needs to first choose a proper Cas9 that is expressed in the
289 precursor cells of the targeted cell population. We show that ubiquitously expressed Cas9 lines,
290 such as *vas-Cas9* (Lopez Del Amo, Juste et al. 2022) and *Act5C-Cas9* (Port, Chen et al. 2014),
291 are sufficient to induce clones in broad tissues. Alternatively, heat shock (HS)-induced Cas9
292 (Garcia-Marques, Espinosa-Medina et al. 2020) can offer temporal control of clone induction in
293 most tissues, akin to the HS-Flp commonly used in FRT-based mosaic analysis. The third option
294 is a Cas9 driven by a tissue-specific enhancer specifically in the precursor cells of the target
295 tissues. Examples shown in this study include *ey-Cas9* expressed in many neuronal lineages (Ji,
296 Sapar et al. 2022), *gcm-Cas9* expressed in glial progenitor cells (Chen, Perry et al. 2024), *zk-*
297 *Cas9* expressed in precursor cells of epidermal cells, motor neurons, and somatosensory neurons
298 (Koreman, Xu et al. 2021), and *hh-Cas9* expressed in imaginal tissues (Poe, Wang et al. 2019).
299 These Cas9 lines have the advantages of being more specific and efficient, and more convenient
300 to use than ubiquitous or inducible ones. Multiple strategies, including enhancer fusion (Port,
301 Chen et al. 2014, Poe, Wang et al. 2019), Gal4-to-Cas9 conversion (Chen, Yao et al. 2020,
302 Koreman, Xu et al. 2021), and insertion of Cas9 in specific gene loci (Chen, Perry et al. 2024),
303 have been developed to ease the generation of such tissue-specific Cas9 lines. As an ongoing
304 effort, we have been converting Gal4 lines known to be expressed in progenitor cells into Cas9
305 (available at https://bdsc.indiana.edu/stocks/genome_editing/crispr_cas9.html), in the hope of
306 making MAGIC accessible to more *Drosophila* tissues. It is worth noting that many Cas9 lines
307 show leaky activity in the germline, which could mutate and inactivate the target sequence in the
308 presence of a gRNA. Thus, it is not recommended to combine Cas9 and gRNA transgenes in the
309 same strain as a long-term stock, unless a Cas9 inhibitor can also be introduced into this stock to
310 suppress the germline activity.

311 The second component of MAGIC is a gRNA-marker line that resides on the appropriate
312 chromosome arm and targets Cas9 to cut a pericentromeric site on the same arm. In the gRNA-
313 marker kit, we generated three lines targeting different sites for each chromosome arm. These
314 lines exhibit a broad range of clone frequencies in larval sensory neurons. As different gRNA-
315 markers maintain similar relative efficiencies of clone induction across tissues (Allen, Koreman
316 et al. 2021), one can choose a gRNA-marker more appropriate for their applications based on the
317 target gene location and the desired clone frequency. Notably, a higher clone frequency may not
318 always be beneficial, such as when studying the projection patterns of individual neurons in the
319 brain. A low efficiency gRNA-marker in this kit may be more desirable in such applications.

320 Besides commonly conducted mosaic analysis in *Drosophila*, MAGIC also enables many
321 novel analyses that are difficult or impossible to accomplish with traditional systems. One
322 example is to analyze interactions among species-specific cells in an interspecific hybrid animal
323 for understanding the cell biological basis of hybrid incompatibility. Interspecific crosses
324 between WT *D. melanogaster* and WT *D. simulans* result in sex-specific lethality of F1 progeny
325 (Barbash 2010). The cellular basis of this lethality is poorly understood. With MAGIC, one may
326 generate mixed cell populations that are homozygous or heterozygous for species-specific alleles
327 in the same hybrid embryo or larva, in which the relative fitness of the three cell populations can
328 be compared. Similarly, MAGIC could complement genome-wide association studies (GWAS)
329 using wild-derived isogenic strains and provide much more mechanistic detail. Such strains as
330 those in the *Drosophila* Genetic Reference Panel (DGRP) (MacKay, Richards et al. 2012) have
331 been very useful for discovering loci that are responsible for phenotypic variations. MAGIC can
332 be combined with these strains to analyze the effects of homozygosity of specific variants at the
333 cell biology level (Allen, Koreman et al. 2021). In addition, MAGIC can be combined with the
334 *Drosophila* deficiency kit for rapid genome-wide mosaic screens. A deficiency exhibiting a
335 desired phenotype in such screens can be further dissected with smaller deficiencies within the
336 deleted region or existing mutations in candidate genes. In this way, the convenience of MAGIC
337 could significantly accelerate phenotype-based gene discovery. Lastly, because the crossover site
338 in MAGIC can be user-defined, one can easily generate gRNA-markers that induce somatic
339 recombination at specific genome locations. With this feature, it is possible to induce crossover
340 between two mutant alleles on the same chromosomal arm to generate clones homozygous for
341 the distal mutation but heterozygous for the proximal mutation. This flexibility could also be

342 useful for mapping undefined genetic loci that are responsible for certain phenotypes, especially
343 in non-traditional model organisms.

344 **MATERIALS AND METHODS:**

345 **Fly Stocks and Husbandry**

346 See the Key Resource Table (Supplementary File 1) for details of fly stocks used in this study.
347 Most fly lines were either generated in the Han lab or obtained from the Bloomington
348 *Drosophila* Stock Center. *lethal hybrid rescue* (*lhr*) mutant *D. Simulans* was a gift from Dr. Dan
349 Barbash. All flies were grown on standard yeast-glucose medium, in a 12:12 light/dark cycle, at
350 25°C unless otherwise noted. Virgin males and females for mating experiments were aged for 3-
351 5 days.

352 To generate and label pMAGIC clones in larval peripheral sensory neurons, we used
353 either *RabX4-Gal4 UAS-MApHS* (for gRNA-markers on chromosomes X, II, and IV) or *21-7-*
354 *Gal4 UAS-MApHS* (for gRNA-markers on chromosome III) combined with *zk-cas9*. To count
355 peripheral sensory neuronal clones on the larval body wall, third instar larvae were mounted
356 laterally on slides and then counted in segment A1-A7 under a Nikon SMZ18 stereomicroscope.
357 pMAGIC clones were induced and labeled by *RabX4-Gal4 UAS-MApHS* combined with *ey-cas9*
358 or *hs-cas9* in the fly adult brain, by *tub-Gal4 UAS-mCD8-GFP* combined with *vas-cas9* in larval
359 brains, imaginal discs, fat bodies, guts, and trachea, by *repo-Gal4 UAS-mCD8-GFP* combined
360 with *gcm-cas9* in glia, by *pxn-Gal4 UAS-tdTom* combined with *Act-cas9* in hemocytes, by *tub-*
361 *Gal4 UAS-mCD8-GFP* combined with *zk-cas9* in larval motor neurons, by *R38F11-Gal4 UAS-*
362 *tdTom* combined with *zk-cas9* in the larval epidermis. To induce nMAGIC clones in wing
363 imaginal discs of interspecific hybrid animals, we use *gRNA-42A4(BFP)*; *hh-cas9* virgin females
364 of *D. melanogaster* to cross with Lhr^1 (Brideau, Flores et al. 2006) *D. simulans* males.

365 **Molecular Cloning**

366 *MAGIC gRNA cloning vectors:* pMAGIC gRNA-marker vectors constructed in this study include
367 pAC-U63-gRNA2.1-ubiGal80(DE)-His2Av, pAC-U63-gRNA2.1-tubGal80(DE)-His2Av and
368 pAC-U63-gRNA2.1-tubGal80(DE)-SV40. To make pAC-U63-gRNA2.1-ubiGal80(DE)-His2Av,
369 a fragment containing gRNA2.1 scaffold (gRNA2.1) and U6 3' flanking sequence (U63fl) was
370 first used to replace gRNA2.1-QtRNA-Gal80(TS)-gRNA2.1-U63fl in pAC-U63-QtgRNA2.1-8R

371 (Addgene 170514) (Koreman, Xu et al. 2021). Then a destabilization sequence (DE) containing a
372 GS linker, amino acids (AAs) 422-461 of mouse ornithine decarboxylase (Zubiaga, Belasco et al.
373 1995), 2X RNA destabilizing nonamer (TTATTTATTgatccTTATTTATT) (Zubiaga, Belasco et
374 al. 1995) was added to the C-terminus of Gal80 in frame. To make pAC-U63-gRNA2.1-
375 tubGal80(DE)-His2Av, a 2.6 kb *tub* enhancer was amplified from pENTR221-tubP (Chen, Wang
376 et al. 2025) by PCR and used to replace the *ubi* enhancer in pAC-U63-gRNA2.1-ubiGal80(DE)-
377 His2Av. To make pAC-U63-gRNA2.1-tubGal80(DE)-SV40, a SV40 polyA sequence was
378 amplified from pAPIC-PHCS (Han, Jan et al. 2011) and used to replace the His2Av polyA in
379 pAC-U63-gRNA2.1-ubiGal80(DE)-His2Av. To make the nMAGIC gRNA-marker vector pAC-
380 U63-gRNA2.1-tubBFP(HA), the gRNA2.1-U63fl fragment was first used to replace gRNA2.1-
381 QtRNA-BFP(TS)-gRNA2.1-U63fl in pAC-U63-QtgRNA2.1-BR (Addgene 170513) (Koreman,
382 Xu et al. 2021). The *tub* enhancer was then used to replace the *ubi* enhancer. Lastly, a synthetic
383 DNA fragment (GenScript) encoding 3X HA was used to replace the nuclear localization signal
384 at the N-terminus of mTagBFP. To make nMAGIC gRNA-marker vector pAC-U63-gRNA2.1-
385 tub-miRFP680-T2A-HO1(HA), an miRFP680-T2A-HO1 coding sequence was used to replace
386 BFP in pAC-U63-gRNA2.1-tubBFP(HA). HO1 encodes haeme oxygenase 1 and is necessary for
387 generating the chromophore of miRFP680. Cloning was carried out by ligation with T4 ligase or
388 NEBuilder DNA Assembly reactions (New England Biolabs Inc.).

389 *MAGIC gRNA expression vectors:* 34 gRNA expression vectors were constructed with the
390 corresponding gRNA cloning vectors as listed in Table 1 according to published protocols
391 (Koreman, Xu et al. 2021). Briefly, for each expression vector, two primers containing
392 appropriate gRNA target sequences (Supplementary File 2) were used to amplify a fragment
393 consisting of 3' end of U6:3 promotor, the first target sequence (TS1), gRNA2.1, $tRNA^{Q}$, the
394 second target sequence (TS2), and the beginning sequence of gRNA2.1 with pAC-U63-
395 QtgRNA2.1-BR as the PCR template. The PCR product was then assembled with SapI-digested
396 gRNA cloning vectors using NEBuilder DNA Assembly.

397 Injections were carried out by Rainbow Transgenic Flies (Camarillo, CA 93012 USA) or
398 Genetivision (Stafford, TX 77477) to transform flies through φC31 integrase-mediated
399 integration into attP docker sites. The 3xP3-RFP selection marker in gRNA-markers inserted at
400 the attP[ZH-102D] site were removed by crossing to Cre.

401 **Live Imaging**

402 Live imaging of larval epidermal cells, sensory neurons, and hemocytes was performed as
403 previously described (Poe, Tang et al. 2017). Animals were collected at 96 (for late third larvae)
404 or 120 h (for wandering third instar larvae) AEL and mounted in glycerol on a slide with vacuum
405 grease as a spacer. Animals were imaged using a Leica SP8 confocal microscope with a 40X
406 NA1.3 oil objective, pinhole size 2 airy units, and a z-step size of 1 μm. For epidermis, images
407 were taken at the dorsal midline of A2 and A3 segments. For dendritic arborization neurons,
408 images were taken from A1 to A7 hemi-segments.

409 For imaging sensory neurons in pupae, newly formed pupae were collected and incubated
410 at 25 °C. After 16 hours, the pupal cases were carefully removed, and the pupae were mounted
411 dorsal side up on slides with halocarbon oil beneath a coverslip. Double-sided tape was used as a
412 spacer. The mounted pupae were imaged using a Leica SP8 confocal microscope with a 40X
413 NA1.3 oil objective.

414 **Heat shock induction of neuronal clones in the adult brain**

415 To induce heat shock, vials containing animals at the appropriate developmental stages were
416 submerged in a 37°C water bath for 1 h. Subsequently, the vials were transferred back to a 25°C
417 incubator until adults emerged.

418 **Imaging of wing discs and other larval tissues**

419 Larval dissections were performed as described previously (Poe, Wang et al. 2019). Briefly,
420 wandering third instar larvae were dissected in a small petri dish filled with cold phosphate-
421 buffered saline (PBS). The anterior half of the larva was inverted. To prepare imaginal discs,
422 trachea and gut were removed. Samples were then transferred to 4% formaldehyde in PBS and
423 fixed for 20 minutes at room temperature. After washing with PBS, the tissues were stained in
424 DAPI (1:1000) in 0.2% PBST (PBS with 0.2% Triton X-100) for 5 minutes. The tissues were
425 washed again in PBST and mounted in SlowFade Diamond Antifade Mountant (Thermo Fisher
426 Scientific) on a glass slide. A coverslip was lightly pressed on top. Imaginal discs were imaged
427 using a Leica SP8 confocal microscope with a 20X NA0.8 oil objective.

428 **Adult brain imaging**

429 Flies were aged for 1 day after eclosion. Brains were dissected in PBS at room temperature and
430 then fixed in 4% paraformaldehyde in PBS with constant circular rotation for 20 minutes at room
431 temperature. The brains were subsequently washed in 0.2% PBST and mounted on a glass slide
432 under a glass coverslip. Vacuum grease was used as a spacer between the coverslip and the slide.
433 Brains were imaged using a Leica SP8 confocal microscope with a 40X NA1.3 oil objective.

434 **Larval fillet preparation**

435 Larval fillet dissection was performed on a petri dish half-filled with PMDS gel. Wandering third
436 instar larvae were pinned on the dish in PBS dorsal-side up and then dissected to expand the
437 body wall. PBS was then removed and 4% formaldehyde in PBS was added to fix larvae for 15
438 minutes at room temperature. For VGlut staining, the fillets were fixed in Bouin's solution for 5
439 minutes at room temperature. Fillets were rinsed and then washed at room temperature in PBS
440 for 20 minutes or until the yellow color from Bouin's solution faded. After immunostaining, the
441 head and tail of fillets were removed, and the remaining fillets were placed in SlowFade
442 Diamond Antifade Mountant on a glass slide. A coverslip was lightly pressed on top. Larval
443 fillets were imaged using a Leica SP8 confocal microscope with a 40X NA1.3 oil objective.

444 **Immunohistochemistry**

445 Larval brains and larval fillets were rinsed and washed at room temperature in 0.2% PBST after
446 fixation. The samples were then blocked in PBST with 5% normal donkey serum (NDS) for 1
447 hour before incubating with appropriate primary antibodies in the blocking solution. Brains were
448 stained for 2 hours at room temperature, and fillets were stained overnight at 4°C. After
449 additional rinsing and washing, the samples were incubated with secondary antibodies for 2
450 hours at room temperature. The samples were then rinsed and washed again before mounting and
451 imaging. Primary antibodies used in this study are mouse anti-Repo antibody 8D12 (1:50
452 dilution), mouse anti-Brp antibody nc82 (1:100 dilution), rabbit anti-VGlut (1:200 dilution)
453 (Chen, Perry et al. 2024), mouse anti-HA antibody (12CA5, 1:100), and goat anti-HRP
454 conjugated with Cy3 (1:200). Secondary antibodies include donkey anti-mouse antibody
455 conjugated with Cy5 (1:400) and donkey anti-rabbit antibody conjugated with Cy5 (1:400).

456 **Image Analysis and Quantification**

ImageJ analyses were conducted in Fiji/ImageJ. To compare brightness of clones in sensory neurons and epidermal cells, clones were detected based on thresholds to generate masks. The clone brightness within the masks was then measured as mean pixel intensity. To quantify clones in wing discs, 2-3 slices of optical sections in the middle of the disc were projected into a 2-dimensional (2D) image. Clones were detected based on a fixed threshold to generate masks, and the total area of clones in the wing pouch of each disc was measured.

The tracing and measurement of da neuron dendrites were done as previously described in detail (Poe, Tang et al. 2017). Briefly, dendrites were segmented using local thresholding. The segments were then converted into single-pixel-width skeletons. The total length of skeletons was calculated based on pixel distance. Normalized dendrite length was calculated as dendritic length (μm)/segment width (μm).

Statistical Analysis

One-way analysis of variance (ANOVA) with Tukey's honest significant difference (HSD) test was used when dependent variable was normally distributed and there was approximately equal variance across groups. Student's t-test or paired t-test was used when two groups are compared. For additional information on the number of samples, see figure legends. R studio was used for all statistical analyses.

ACKNOWLEDGMENTS

We thank Dion Dickman, Marcus Smolka, and Developmental Studies Hybridoma Bank (DSHB) for antibodies; Dan Barbash, Ethan Bier, and Bloomington *Drosophila* Stock Center for fly stocks; Dan Barbash and Tianzhu Xiong for advice on interspecific crosses; Claire Ho and Christina Breneman for helping to establish and test transgenes; Dan Barbash and Mariana Wolfner for feedback on the manuscript.

AUTHOR CONTRIBUTIONS

Conceptualization: Chun Han, Yifan Shen, Ann Yeung

Data curation: Yifan Shen, Ann Yeung, Elizabeth Korn, Rhiannon Clements, Parker Jarman

Formal analysis: Yifan Shen, Ann Yeung, Rhiannon Clements

Funding acquisition: Chun Han

485 **Investigation:** Yifan Shen, Ann Yeung, Elizabeth Korn, Rhiannon Clements, Xinchen Chen,
486 Zixian Huang, Michael Sheen, Parker Jarman

487 **Methodology:** Chun Han, Yifan Shen, Ann Yeung

488 **Supervision:** Chun Han, Yifan Shen, Ann Yeung, Rhiannon Clements, Elizabeth Korn

489 **Resources:** Yifan Shen, Payton Ditchfield, Bei Wang

490 **Validation:** Yifan Shen

491 **Visualization:** Yifan Shen, Ann Yeung, Rhiannon Clements

492 **Writing – original draft:** Chun Han, Yifan Shen

493 **Writing – review & editing:** Chun Han, Yifan Shen

494 **DATA AVAILABILITY**

495 All data generated or analyzed during this study are included in the manuscript and supporting
496 files. The MAGIC gRNA-marker fly stocks generated in this study have been deposited to the
497 Bloomington *Drosophila* Stock Center. Plasmids have been deposited to Addgene.

498 **REFERENCES**

499 Allen, S. E., G. T. Koreman, A. Sarkar, B. Wang, M. F. Wolfner and C. Han (2021). "Versatile
500 CRISPR/Cas9-mediated mosaic analysis by gRNA-induced crossing-over for unmodified
501 genomes." PLoS Biol **19**(1): e3001061.

502 Barbash, D. A. (2010). "Ninety years of Drosophila melanogaster hybrids." Genetics **186**(1): 1-8.

503 Bellen, H. J., R. W. Levis, Y. He, J. W. Carlson, M. Evans-Holm, E. Bae, J. Kim, A. Metaxakis,
504 C. Savakis, K. L. Schulze, R. A. Hoskins and A. C. Spradling (2011). "The Drosophila gene
505 disruption project: progress using transposons with distinctive site specificities." Genetics
506 **188**(3): 731-743.

507 Bellen, H. J., R. W. Levis, G. Liao, Y. He, J. W. Carlson, G. Tsang, M. Evans-Holm, P. R.
508 Hiesinger, K. L. Schulze, G. M. Rubin, R. A. Hoskins and A. C. Spradling (2004). "The BDGP
509 gene disruption project: single transposon insertions associated with 40% of Drosophila genes."
510 Genetics **167**(2): 761-781.

511 Brideau, N. J., H. A. Flores, J. Wang, S. Maheshwari, X. Wang and D. A. Barbash (2006). "Two
512 Dobzhansky-Muller genes interact to cause hybrid lethality in Drosophila." Science **314**(5803):
513 1292-1295.

514 Brown, H. L., L. Cherbas, P. Cherbas and J. W. Truman (2006). "Use of time-lapse imaging and
515 dominant negative receptors to dissect the steroid receptor control of neuronal remodeling in
516 Drosophila." Development **133**(2): 275-285.

Chakraborty, M., C. H. Chang, D. E. Khost, J. Vedanayagam, J. R. Adrion, Y. Liao, K. L. Montooth, C. D. Meiklejohn, A. M. Larracuente and J. J. Emerson (2021). "Evolution of genome structure in the Drosophila simulans species complex." Genome Res **31**(3): 380-396.

Charng, W. L., S. Yamamoto and H. J. Bellen (2014). "Shared mechanisms between Drosophila peripheral nervous system development and human neurodegenerative diseases." Curr Opin Neurobiol **27**: 158-164.

Chen, H. M., X. Yao, Q. Ren, C. C. Chang, L. Y. Liu, R. L. Miyares and T. Lee (2020). "Enhanced Golic+: highly effective CRISPR gene targeting and transgene HACKing in Drosophila." Development **147**(11).

Chen, X., S. Perry, Z. Fan, B. Wang, E. Loxterkamp, S. Wang, J. Hu, D. Dickman and C. Han (2024). "Tissue-specific knockout in the Drosophila neuromuscular system reveals ESCRT's role in formation of synapse-derived extracellular vesicles." PLoS Genet **20**(10): e1011438.

Chen, X., B. Wang, A. Sarkar, Z. Huang, N. V. Ruiz, A. T. Yeung, R. Chen and C. Han (2025). "Phagocytosis-driven neurodegeneration through opposing roles of an ABC transporter in neurons and phagocytes." Sci Adv **11**(11): eadr5448.

Chou, V. T., S. A. Johnson and D. Van Vactor (2020). "Synapse development and maturation at the drosophila neuromuscular junction." Neural Dev **15**(1): 11.

Cook, R. K., S. J. Christensen, J. A. Deal, R. A. Coburn, M. E. Deal, J. M. Gresens, T. C. Kaufman and K. R. Cook (2012). "The generation of chromosomal deletions to provide extensive coverage and subdivision of the Drosophila melanogaster genome." Genome Biol **13**(3): R21.

Daniels, R. W., C. A. Collins, M. V. Gelfand, J. Dant, E. S. Brooks, D. E. Krantz and A. DiAntonio (2004). "Increased expression of the Drosophila vesicular glutamate transporter leads to excess glutamate release and a compensatory decrease in quantal content." J Neurosci **24**(46): 10466-10474.

Garcia-Marques, J., I. Espinosa-Medina, K.-Y. Ku, C.-P. Yang, M. Koyama, H.-H. Yu and T. Lee (2020). "A programmable sequence of reporters for lineage analysis." Nature Neuroscience.

Germani, F., C. Bergantinos and L. A. Johnston (2018). "Mosaic Analysis in Drosophila." Genetics **208**: 4733-4490.

Goldsmith, S. L., M. Shimell, P. Tauscher, S. M. Daly, O. Shimmi, M. B. O'Connor and S. J. Newfeld (2022). "New resources for the Drosophila 4th chromosome: FRT101F enabled mitotic clones and Bloom syndrome helicase enabled meiotic recombination." G3 (Bethesda) **12**(4).

Golic, K. G. and S. Lindquist (1989). "The FLP recombinase of yeast catalyzes site-specific recombination in the Drosophila genome." Cell **59**(3): 499-509.

Griffin, R., R. Binari and N. Perrimon (2014). "Genetic odyssey to generate marked clones in Drosophila mosaics." Proc Natl Acad Sci U S A **111**(13): 4756-4763.

Hacker, U., S. Nystedt, M. P. Barmchi, C. Horn and E. A. Wimmer (2003). "piggyBac-based insertional mutagenesis in the presence of stably integrated P elements in Drosophila." Proc Natl Acad Sci U S A **100**(13): 7720-7725.

556 Han, C., L. Y. Jan and Y. N. Jan (2011). "Enhancer-driven membrane markers for analysis of
557 nonautonomous mechanisms reveal neuron-glia interactions in Drosophila." Proc Natl Acad Sci
558 U S A **108**(23): 9673-9678.

559 Han, C., Y. Song, H. Xiao, D. Wang, N. C. Franc, L. Y. Jan and Y. N. Jan (2014). "Epidermal
560 cells are the primary phagocytes in the fragmentation and clearance of degenerating dendrites in
561 Drosophila." Neuron **81**(3): 544-560.

562 Henner, A., P. B. Ventura, Y. Jiang and H. Zong (2013). "MADM-ML, a mouse genetic mosaic
563 system with increased clonal efficiency." PLoS One **8**(10): e77672.

564 Ji, H., M. L. Sapar, A. Sarkar, B. Wang and C. Han (2022). "Phagocytosis and self-destruction
565 break down dendrites of Drosophila sensory neurons at distinct steps of Wallerian degeneration."
566 Proc Natl Acad Sci U S A **119**(4).

567 Kittel, R. J., C. Wichmann, T. M. Rasse, W. Fouquet, M. Schmidt, A. Schmid, D. A. Wagh, C.
568 Pawlu, R. R. Kellner, K. I. Willig, S. W. Hell, E. Buchner, M. Heckmann and S. J. Sigrist (2006).
569 "Bruchpilot promotes active zone assembly, Ca2+ channel clustering, and vesicle release."
570 Science **312**(5776): 1051-1054.

571 Koreman, G. T., Y. Xu, Q. Hu, Z. Zhang, S. E. Allen, M. F. Wolfner, B. Wang and C. Han (2021).
572 "Upgraded CRISPR/Cas9 tools for tissue-specific mutagenesis in Drosophila." Proc Natl Acad
573 Sci U S A **118**(14).

574 Lee, T. and L. Luo (1999). "Mosaic analysis with a repressible cell marker for studies of gene
575 function in neuronal morphogenesis." Neuron **22**(3): 451-461.

576 Li, X., X. Zhao, Y. Fang, X. Jiang, T. Duong, C. Fan, C. C. Huang and S. R. Kain (1998).
577 "Generation of destabilized green fluorescent protein as a transcription reporter." J Biol Chem
578 **273**(52): 34970-34975.

579 Lopez Del Amo, V., S. S. Juste and V. M. Gantz (2022). "A nickase Cas9 gene-drive system
580 promotes super-Mendelian inheritance in Drosophila." Cell Rep **39**(8): 110843.

581 MacKay, T. F. C., S. Richards, E. A. Stone, A. Barbadilla, J. F. Ayroles, D. Zhu, S. Casillas, Y.
582 Han, M. M. Magwire, J. M. Cridland, M. F. Richardson, R. R. H. Anholt, M. Barrón, C. Bess, K.
583 P. Blankenburg, M. A. Carbone, D. Castellano, L. Chaboub, L. Duncan, Z. Harris, M. Javaid, J.
584 C. Jayaseelan, S. N. Jhangiani, K. W. Jordan, F. Lara, F. Lawrence, S. L. Lee, P. Librado, R. S.
585 Linheiro, R. F. Lyman, A. J. MacKey, M. Munidasa, D. M. Muzny, L. Nazareth, I. Newsham, L.
586 Perales, L. L. Pu, C. Qu, M. Ràmia, J. G. Reid, S. M. Rollmann, J. Rozas, N. Saada, L. Turlapati,
587 K. C. Worley, Y. Q. Wu, A. Yamamoto, Y. Zhu, C. M. Bergman, K. R. Thornton, D. Mittelman
588 and R. A. Gibbs (2012). "The Drosophila melanogaster Genetic Reference Panel." Nature
589 **482**(7384): 173-178.

590 Matlashov, M. E., D. M. Shcherbakova, J. Alvelid, M. Baloban, F. Pennacchietti, A. A.
591 Shemetov, I. Testa and V. V. Verkhusha (2020). "A set of monomeric near-infrared fluorescent
592 proteins for multicolor imaging across scales." Nat Commun **11**(1): 239.

593 Menon, K. P., R. A. Carrillo and K. Zinn (2013). "Development and plasticity of the Drosophila
594 larval neuromuscular junction." Wiley Interdiscip Rev Dev Biol **2**(5): 647-670.

595 Poe, A. R., L. Tang, B. Wang, Y. Li, M. L. Sapar and C. Han (2017). "Dendritic space-filling
596 requires a neuronal type-specific extracellular permissive signal in Drosophila." PNAS: E8062-
597 E8071.

598 Poe, A. R., B. Wang, M. L. Sapar, H. Ji, K. Li, T. Onabajo, R. Fazliyeva, M. Gibbs, Y. Qiu, Y. Hu
599 and C. Han (2019). "Robust CRISPR/Cas9-Mediated Tissue-Specific Mutagenesis Reveals Gene
600 Redundancy and Perdurance in Drosophila." Genetics **211**(2): 459-472.

601 Port, F., H. M. Chen, T. Lee and S. L. Bullock (2014). "Optimized CRISPR/Cas tools for
602 efficient germline and somatic genome engineering in Drosophila." PNAS **111**(29): E2967-
603 E2976.

604 Riddle, N. C., A. Minoda, P. V. Kharchenko, A. A. Alekseyenko, Y. B. Schwartz, M. Y.
605 Tolstorukov, A. A. Gorchakov, J. D. Jaffe, C. Kennedy, D. Linder-Basso, S. E. Peach, G.
606 Shanower, H. Zheng, M. I. Kuroda, V. Pirrotta, P. J. Park, S. C. Elgin and G. H. Karpen (2011).
607 "Plasticity in patterns of histone modifications and chromosomal proteins in Drosophila
608 heterochromatin." Genome Res **21**(2): 147-163.

609 Staudt, N., A. Molitor, K. Somogyi, J. Mata, S. Curado, K. Eulenberg, M. Meise, T. Siegmund, T.
610 Hader, A. Hilfiker, G. Bronner, A. Ephrussi, P. Rorth, S. M. Cohen, S. Fellert, H. R. Chung, O.
611 Piepenburg, U. Schafer, H. Jackle and G. Vorbruggen (2005). "Gain-of-function screen for genes
612 that affect Drosophila muscle pattern formation." PLoS Genet **1**(4): e55.

613 Thibault, S. T., M. A. Singer, W. Y. Miyazaki, B. Milash, N. A. Dompe, C. M. Singh, R.
614 Buchholz, M. Demsky, R. Fawcett, H. L. Francis-Lang, L. Ryner, L. M. Cheung, A. Chong, C.
615 Erickson, W. W. Fisher, K. Greer, S. R. Hartouni, E. Howie, L. Jakkula, D. Joo, K. Killpack, A.
616 Laufer, J. Mazzotta, R. D. Smith, L. M. Stevens, C. Stuber, L. R. Tan, R. Ventura, A. Woo, I.
617 Zakrajsek, L. Zhao, F. Chen, C. Swimmer, C. Kopczynski, G. Duyk, M. L. Winberg and J.
618 Margolis (2004). "A complementary transposon tool kit for Drosophila melanogaster using P and
619 piggyBac." Nat Genet **36**(3): 283-287.

620 Wagh, D. A., T. M. Rasse, E. Asan, A. Hofbauer, I. Schwenkert, H. Durrbeck, S. Buchner, M. C.
621 Dabauvalle, M. Schmidt, G. Qin, C. Wichmann, R. Kittel, S. J. Sigrist and E. Buchner (2006).
622 "Bruchpilot, a protein with homology to ELKS/CAST, is required for structural integrity and
623 function of synaptic active zones in Drosophila." Neuron **49**(6): 833-844.

624 Williams, D. W. and J. W. Truman (2005). "Cellular mechanisms of dendrite pruning in
625 Drosophila: insights from in vivo time-lapse of remodeling dendritic arborizing sensory
626 neurons." Development **132**(16): 3631-3642.

627 Xu, T. and G. M. Rubin (1993). "Analysis of genetic mosaics in developing and adult Drosophila
628 tissues." Development **117**(4): 1223-1237.

629 Xu, T. and G. M. Rubin (2012). "The effort to make mosaic analysis a household tool."
630 Development **139**(24): 4501-4503.

631 Yamamoto, S., M. Jaiswal, W. L. Charng, T. Gambin, E. Karaca, G. Mirzaa, W. Wiszniewski, H.
632 Sandoval, N. A. Haelterman, B. Xiong, K. Zhang, V. Bayat, G. David, T. Li, K. Chen, U. Gala, T.
633 Harel, D. Pehlivan, S. Penney, L. Vissers, J. de Ligt, S. N. Jhangiani, Y. Xie, S. H. Tsang, Y.
634 Parman, M. Sivaci, E. Battaloglu, D. Muzny, Y. W. Wan, Z. Liu, A. T. Lin-Moore, R. D. Clark, C.
635 J. Curry, N. Link, K. L. Schulze, E. Boerwinkle, W. B. Dobyns, R. Allikmets, R. A. Gibbs, R.

636 Chen, J. R. Lupski, M. F. Wangler and H. J. Bellen (2014). "A drosophila genetic resource of
637 mutants to study mechanisms underlying human genetic diseases." Cell **159**(1): 200-214.

638 Zong, H., J. S. Espinosa, H. H. Su, M. D. Muzumdar and L. Luo (2005). "Mosaic Analysis with
639 Double Markers in Mice." Cell **121**(3): 479-492.

640 Zubiaga, A. M., J. G. Belasco and M. E. Greenberg (1995). "The nonamer UUAUUUAUU is the
641 key AU-rich sequence motif that mediates mRNA degradation." Mol Cell Biol **15**(4): 2219-2230.

642

643

644 **FIGURE**

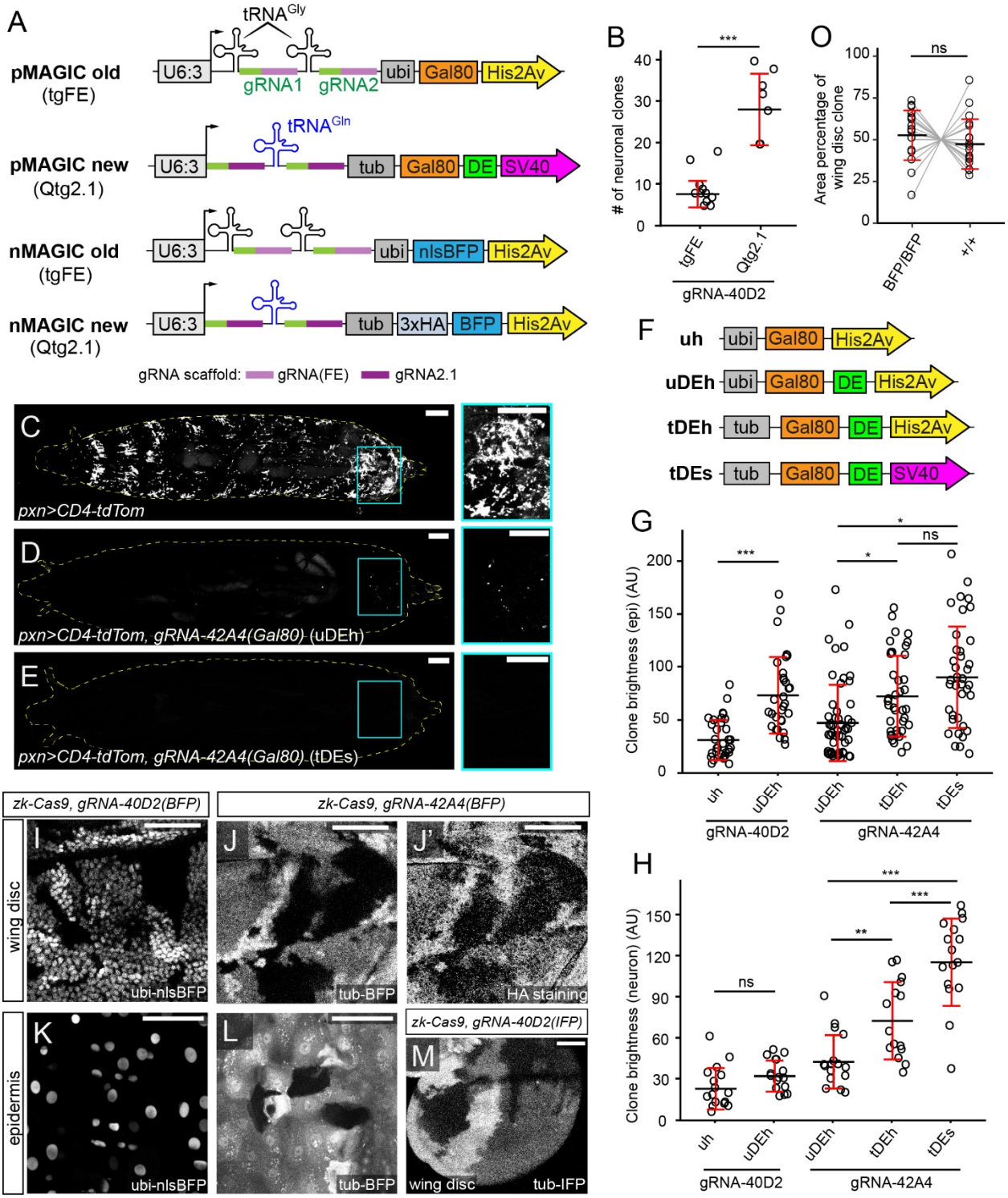

645

646 **Figure 1. New gRNA-marker designs improve pMAGIC and nMAGIC.**

(A) Original and new designs of gRNA-markers for pMAGIC and nMAGIC. (B) Comparison of clone frequency in larval sensory neurons between two gRNA designs. Clones were induced by *zk-Cas9* (expressed in the embryonic ectoderm) and labeled by the pan-neuronal driver *RabX4-Gal4>MApHS* (MApHS: pHluorin-CD4-tdTomato). The number represents clones between A1 and A7 segments on one side of each larva. n = larvae number: tgFE (n=10), Qtg2.1 (n=10). (C-E) Labeling of hemocytes in whole 3rd instar larvae by *pxn-Gal4>CD4-tdTom* alone (C) or together with *gRNA-42A4(Gal80)-uDEH* (*ubi-Gal80)* (D) or *gRNA-42A4(Gal80)-tDES* (*tub-Gal80*) (E). The panels on the right show enlarged views of the boxed regions. (F) Designs of Gal80 variants tested in pMAGIC gRNA-markers. (G) The brightness of epidermal clones induced by *zk-Cas9* and labeled by the epidermal driver *R38F11-Gal4>tdTom* in the presence of pMAGIC gRNA-markers. n = image numbers: gRNA-40D2-uH (n = 32), gRNA-40D2-uDEH (n = 31), gRNA-42A4-uDEH (n = 52), gRNA-42A4-tDEH (n = 39), gRNA-42A4-tDES (n = 38). (H) The brightness of neuronal clones induced by *zk-Cas9* and labeled by *RabX4-Gal4>MApHS* in the presence of pMAGIC gRNA-markers. The brightness of tdTom was measured and compared. n = neuron numbers: gRNA-40D2-uH (n = 16), gRNA-40D2-uDEH (n = 16), gRNA-42A4-uDEH (n = 16), gRNA-42A4-tDEH (n = 15), gRNA-42A4-tDES (n = 16). (I) A portion of a larval wing disc containing nMAGIC clones visualized by nlsBFP. (J and J') A portion of a wing disc containing nMAGIC clones labeled by cytosolic BFP (J) and HA staining (J'). (K) Epidermal clones on the larva body wall labeled by nlsBFP. (L) Epidermal clones visualized by cytosolic BFP. (M) A portion of a wing disc containing nMAGIC clones labeled by cytosolic miRFP680 (IFP). (O) Sizes of nMAGIC *BFP/BFP* clones and wildtype (+/+) clones in wing discs. Two types of clones in the same discs were connected. n = wing disc number: BFP/BFP (n = 18), +/+ (n=18). In all plots, black bar, mean; red bar, SD; AU, arbitrary unit. Student's t-test in (B); one-way analysis of variance (ANOVA) and Tukey's honest significant difference (HSD) test in (G) and (H). paired t-test in (O) *$p \leq 0.05$, **$p \leq 0.01$, ***$p \leq 0.001$, ns, not significant. For (C-E), scale bar, 300 µm. For (I-M), scale bar, 100 µm.

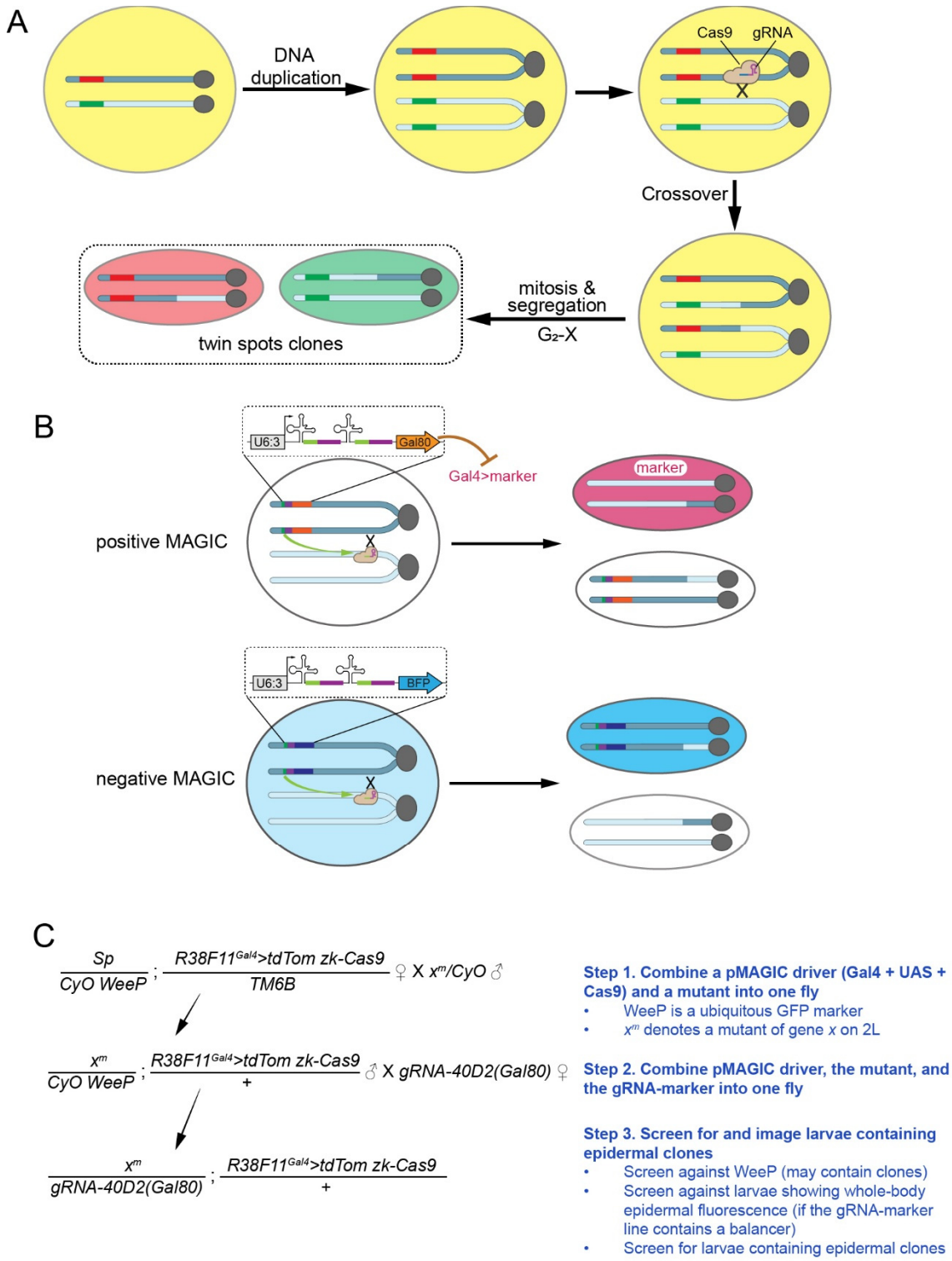

673

674 **Figure 1 – figure supplement 1. MAGIC principles.**

675 (A) A diagram of MAGIC principle. This diagram is based on a hypothetic cell that contains a

676 GFP (green) marker and an RFP (red) marker on two homologous chromosomes. Co-existence of

677 the two markers render the cell yellow, while their segregation through mitotic recombination
678 results in red-only and green-only twin-spot daughter cells. (B) Diagrams of positive MAGIC
679 (pMAGIC) and negative MAGIC (nMAGIC). pMAGIC involves ubiquitously expressed Gal80
680 that suppresses Gal4-driven expression of a fluorescent marker in Gal80-containing cells. Only
681 homozygous cells lacking the gRNA-marker will be labeled. nMAGIC utilizes ubiquitously
682 expressed BFP to distinguish two populations of twin-spot cells, one with two copies of BFP and
683 the other lacking BFP entirely. (C) An example crossing scheme of pMAGIC experiments. This
684 example uses the epidermal *R38F11-Gal4* to drive expression of tdTom and the
685 epidermal/neuronal progenitor *zk-Cas9* to induce clones. For the convenience of the experiment,
686 R38F11-Gal4, UAS-tdTom, and zk-Cas9 have been recombined onto the same chromosome.

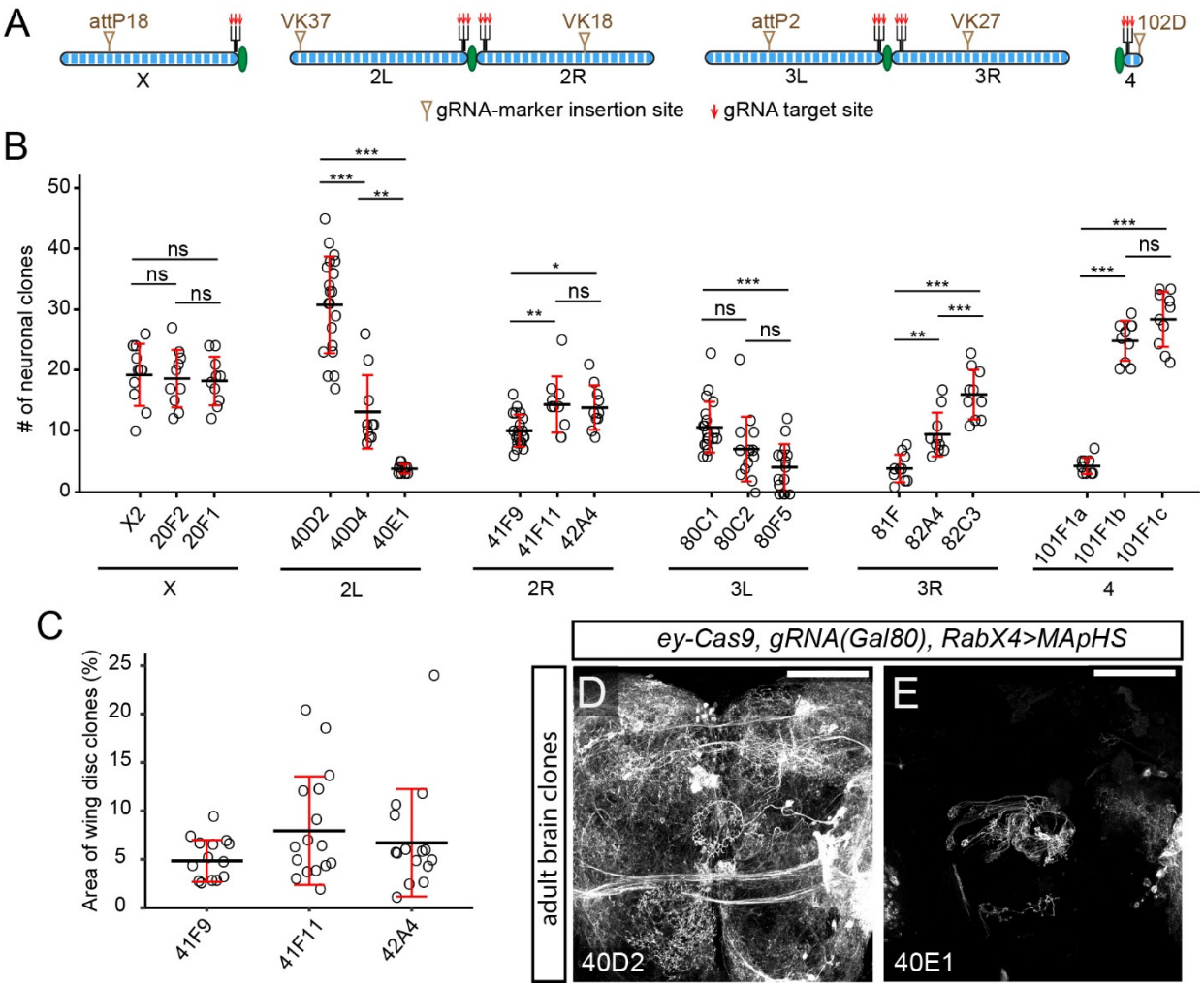

687

688 **Figure 2. A genome-wide gRNA-marker kit suits diverse needs of clone frequency.**

689 (A) Scheme of gRNA-marker insertion sites and target sites on *Drosophila* chromosomes. (B)
690 Comparison of clone frequencies of all pMAGIC gRNA-markers in larval sensory neurons,
691 clones are labeled using *RabX4-Gal4>MApHs* (for Chromosome X, II and IV) or *21-7-Gal4*
692 *UAS-MApHS* (for Chromosome III). n = larvae number: X2 (n = 10), 20F2 (n = 10), 20F1(n =
693 10), 40D2 (n = 20), 40D4 (n = 10), 40E1 (n = 10), 41F9 (n = 20), 41F11 (n = 10), 42A4 (n =
694 10), 80C1 (n = 20), 80C2 (n = 14), 80F5 (n = 15), 81F (n = 10), 82A4 (n = 10), 82C3 (n = 10),
695 101F1a (n = 10), 101F1b (n = 10), 101F1c (n = 10). (C) Comparison of clone areas in larval
696 wing discs labeled by nMAGIC gRNA-markers on 2R. n = wing disc number: 41F9 (n = 14),
697 41F11 (n = 16), 42A4 (n = 15). (D and E) Neuronal clones in the central part of the adult brain
698 induced by *ey-Cas9* (expressed in progenitor cells of many neuronal tissues) and labeled by
699 *RabX4-Gal4>MApHS* along with pMAGIC gRNA-markers *gRNA-40D2* (D) and *gRNA-40E1*
700 (E). MApHS contains pHluorin and tdTom (Han, Song et al. 2014), but only the tdTom channel
701 is shown. In all plots, black bar, mean; red bar, SD. One-way ANOVA and Tukey's HSD test.
702 *$p \leq 0.05$, **$p \leq 0.01$, ***$p \leq 0.001$, ns, not significant. For (D) and (E), scale bar 100 μm.

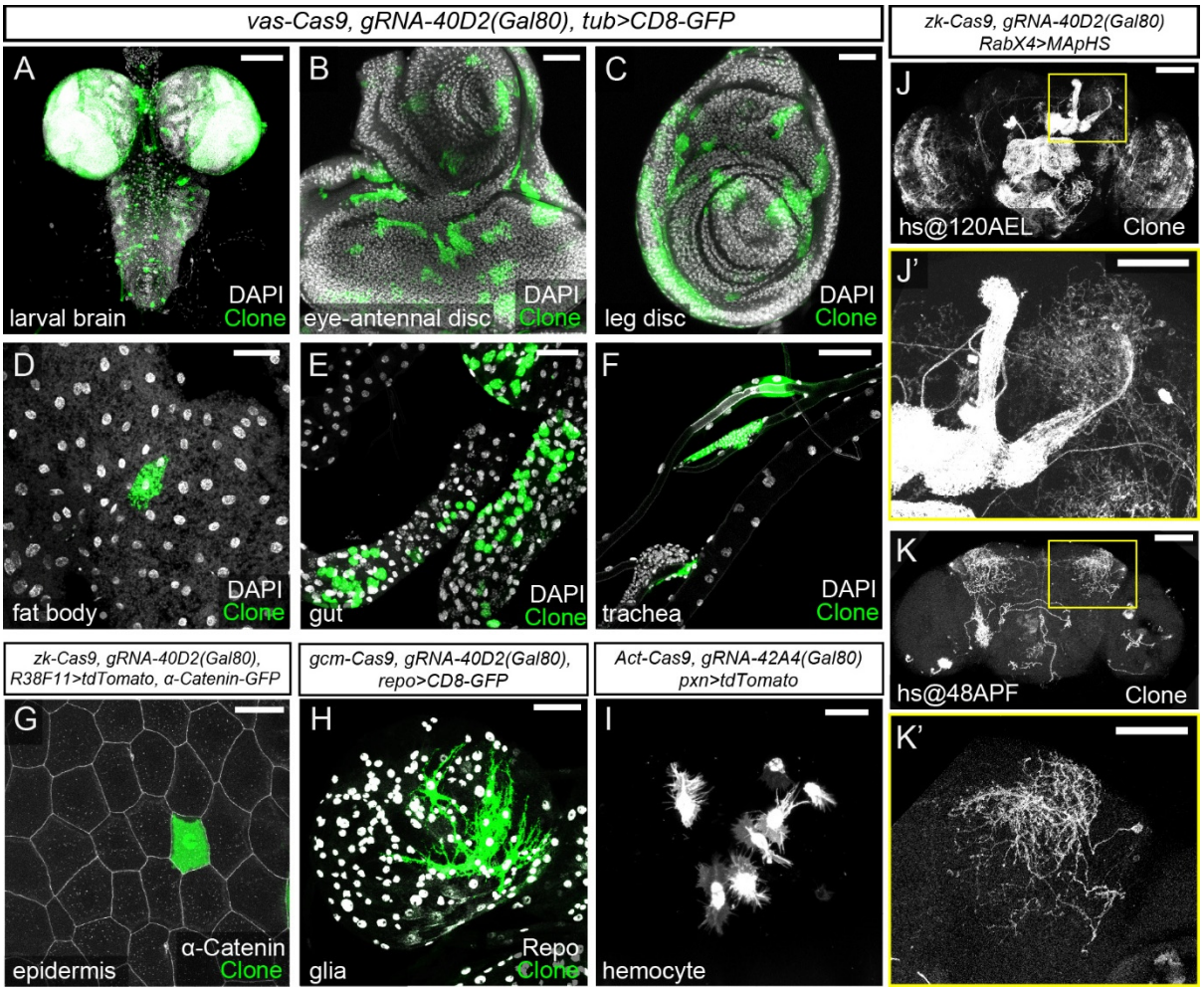

Figure 3. MAGIC allows clonal analysis in diverse tissues and cell types.

(A-F) pMAGIC clones induced in different tissues by *vas-Cas9* (ubiquitous Cas9) *gRNA-40D2(Gal80)* and labeled by *tub-Gal4 UAS-CD8-GFP* (green). DAPI staining (white) shows all nuclei. (G) A pMAGIC epidermal clone on the larval body wall induced by *zk-Cas9 gRNA-40D2(Gal80)* and labeled by *R38F11-Gal4>tdTom* (green). Epidermal junctions are labeled by *α-Catenin-GFP* (white). (H) pMAGIC glia clones in the larval brain induced by *gcm-Cas9* (expressed in glial precursor genes) *gRNA-40D2(Gal80)* and labeled by *repo-Gal4 UAS-CD8-GFP* (green). Glial nuclei are labeled by Repo staining (white). (I) pMAGIC hemocyte clones induced by *Act-Cas9 gRNA-40D2(Gal80)* and labeled by *pxn-Gal4>CD4-tdTom*. (J-K') pMAGIC clones in adult brain induced by *hs-Cas9 gRNA-40D2(Gal80)* and labeled by *RabX4-Gal4>MApHS.* Heat shock was performed at 120 h after egg lay (AEL) (J-J') and 48 h after puparium formation (APF) (K-K'). The boxed areas were enlarged to show clones in the

716 mushroom body and lateral horn region. Only the tdTom channel is shown. In (A), (D-F), (H),
717 (J), and (K), scale bar 100 µm; in (B-C), (G), (J'), and (K'), scale bar 50 µm; in (I), scale bar 25
718 µm.

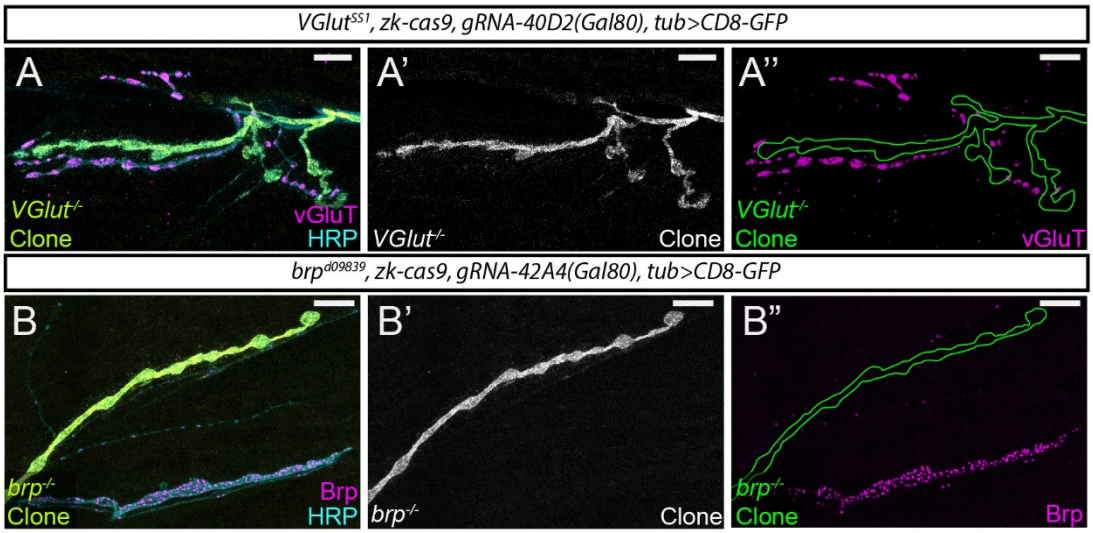

719

720 **Figure 4. MAGIC facilitates clonal analysis at the NMJ.**

721 (A-A") pMAGIC clones of *VGlut*^{1} mutation in motor neurons at the neuromuscular junction.
722 Clones were induced by *zk-Cas9 gRNA-40D2(Gal80)* and labeled by *tub-Gal4>CD8-GFP*. The
723 loss of VGlut is confirmed by VGlut staining. The mutant clones are outlined in (A"). (B-B") A
724 pMAGIC clone of *brp*^{d09839} mutation in a motor neuron at the neuromuscular junction. Clones
725 were induced by *zk-Cas9 gRNA-42A4(Gal80)* and labeled by *tub-Gal4>CD8-GFP*. The loss of
726 Brp is confirmed by Brp staining. The mutant clone is outlined in (B"). In both experiments,
727 HRP staining shows all axons. Scale bars, 10 µm.

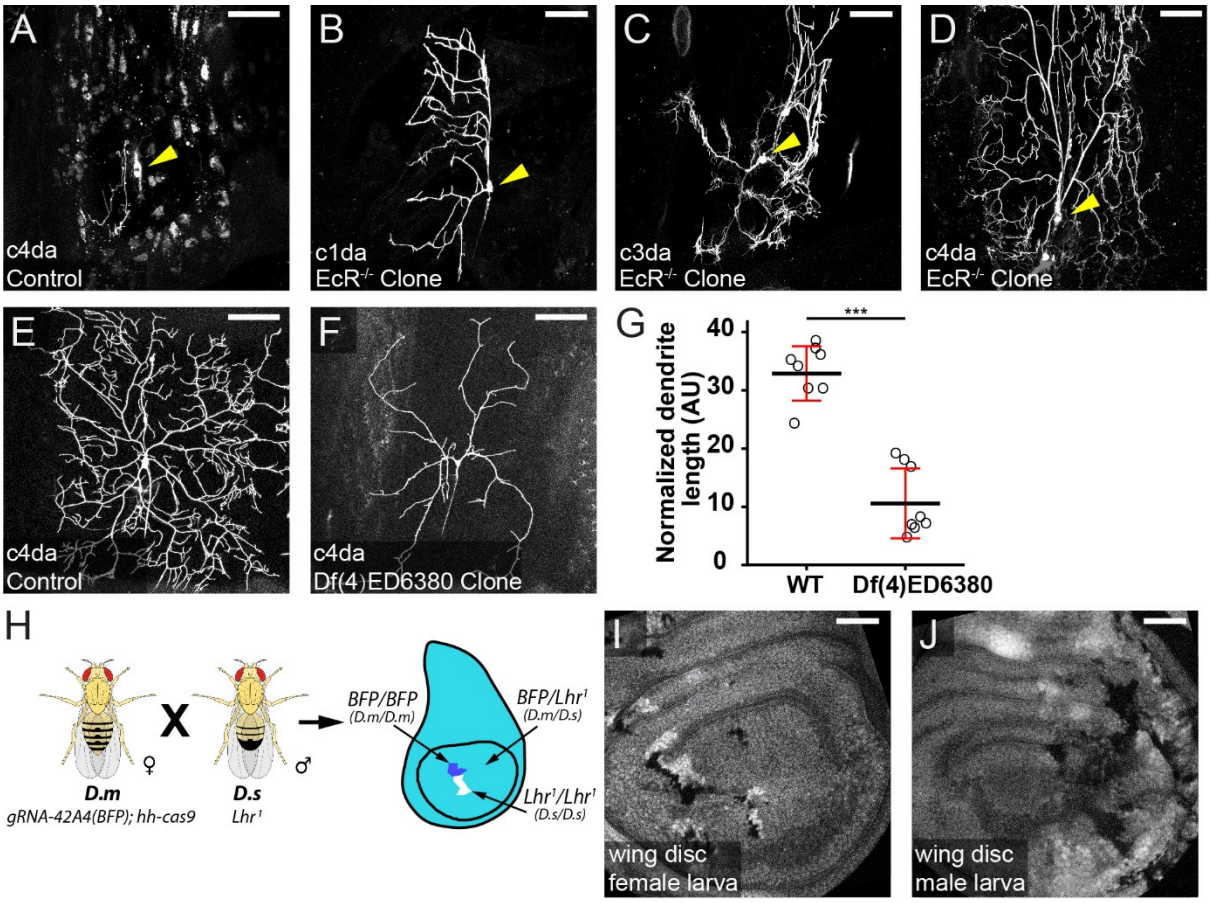

Figure 5. MAGIC enables clonal analysis of pericentromeric genes, 4th chromosome-associated mutations, and in interspecific hybrid animals.

(A) A WT pMAGIC class IV da neuron clone exhibiting complete dendrite pruning at 16 hours APF. (B-D) pMAGIC clones of *EcR*^{M554fs} mutation in da neurons imaged at 16 hours APF, exhibiting the lack of pruning (B and D) or apoptosis (C). In (A-D), the clones were induced by *zk-cas9* with *gRNA-41F9(Gal80)* and labeled by *RabX4-Gal4>MApHS*. Neuronal cell bodies are indicated by arrows. Only the tdTom channel is shown. The signals in epidermal cells (A) were due to engulfment of pruned dendrites by epidermal cells (Han, Song et al. 2014). (E and F) WT (E) and *Df(4)ED6380* (F) pMAGIC clones in C4da neurons induced by *zk-cas9 gRNA-101Fc(Gal80)* and labeled by *RabX4-Gal4>MApHS*. Only the tdTom channel is shown. (G) Normalized dendrite length of WT clones and deficiency clones. Black bar, mean; red bar, SD. Student's t-test. ***$p \leq 0.001$. (H) Scheme for interspecific crosses between *D. melanogaster* (*D.m*) and *D. simulans* (*D.s*). (I and J) Wing discs from male (I) and female (J) progeny carrying clones. Scale bars, 50 µm.

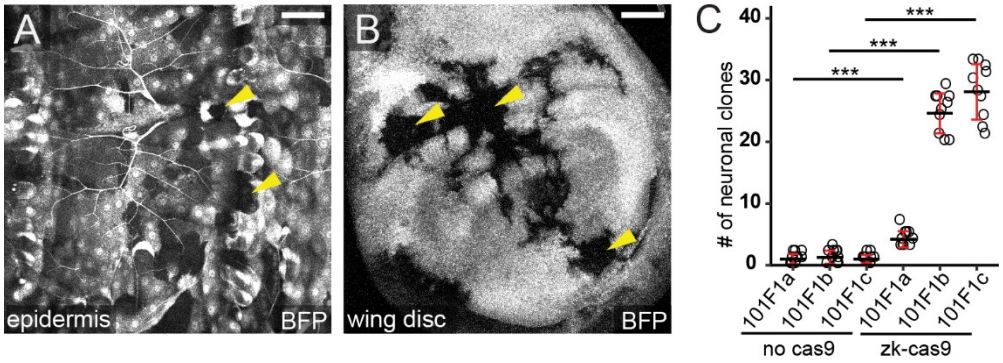

743

744 **Figure 5 – figure supplement 1. Transgenic markers on the 4th chromosome show uneven**
745 **expression.**

746 (A-B) Representative epidermal (A) and wing disc (B) images showing uneven expression of
747 *gRNA-101F1c(BFP)* inserted at *attP*^{102D} on the 4th chromosome. Yellow arrowheads point to cells
748 lacking BFP expression. Scale bars, 50 µm. (C) Frequency of labeled neurons by indicated
749 gRNA(Gal80) in the absence and presence of Cas9. The *zk-Cas9* dataset is the same as that for
750 chromosome 4 in Figure 2B. Black bar, mean; red bar, SD. One-way ANOVA and HSD test.
751 ***p≤0.001.

752 **Table 1. gRNA-marker collection**

Chr Arm	target site	gRNA location	pMAGIC vector	nMAGIC vector	clone frequency	BDSC IDs***
2L	40D2	attP[VK00037]	*pAC-U63-gRNA2.1-ubiGal80(DE)-His2Av*	*pAC-U63-tgRNA-nlsBFP** *pAC-U63-gRNA2.1-tub-miRFP680-T2A-HO1(HA) (HA)*	31	606005 & 92741
2L	40D4	attP[VK00037]	*pAC-U63-tgRNA-Gal80**	*pAC-U63-tgRNA-nlsBFP**	13	92744 & 92742
2L	40E1	attP[VK00037]	*pAC-U63-tgRNA-Gal80**	*pAC-U63-tgRNA-nlsBFP**	4	606004 & 606003
2R	41F9	attP[VK00018]	*pAC-U63-gRNA2.1-ubiGal80(DE)-His2Av*	*pAC-U63-gRNA2.1-tubBFP(HA)*	10	606006 &

						606010
2R	41F11	attP[VK00018]	*pAC-U63-gRNA2.1-ubiGal80(DE)-His2Av*	*pAC-U63-gRNA2.1-tubBFP(HA)*	14	606007 & 606009
2R	42A4	attP[VK00018]	*pAC-U63-gRNA2.1-tubGal80(DE)-SV40*	*pAC-U63-gRNA2.1-tubBFP(HA)*	14	606008 & 606011
3L	80F5	attP2	*pAC-U63-gRNA2.1-tubGal80(DE)-His2Av*	*pAC-U63-gRNA2.1-tubBFP(HA)*	11	606014 & 606017
3L	80C2	attP2	*pAC-U63-gRNA2.1-tubGal80(DE)-His2Av*	*pAC-U63-gRNA2.1-tubBFP(HA)*	7	606013 & 606016
3L	80C1	attP2	*pAC-U63-gRNA2.1-tubGal80(DE)-His2Av*	*pAC-U63-gRNA2.1-tubBFP(HA)*	4	606012 & 606015
3R	81F	attP[VK00027]	*pAC-U63-gRNA2.1-tubGal80(DE)-His2Av*	*pAC-U63-gRNA2.1-tubBFP(HA)*	4	606020 & 606021
3R	82A4	attP[VK00027]	*pAC-U63-gRNA2.1-tubGal80(DE)-His2Av*	*pAC-U63-gRNA2.1-tubBFP(HA)*	10	606018 & 606022
3R	82C3	attP[VK00027]	*pAC-U63-gRNA2.1-tubGal80(DE)-His2Av*	*pAC-U63-gRNA2.1-tubBFP(HA)*	16	606019 & 606023
X	X2	attP18	*pAC-U63-gRNA2.1-tubGal80(DE)-SV40*	*pAC-U63-gRNA2.1-tubBFP(HA)*	19	606024 & 606028

X	20F1	attP18	*pAC-U63-gRNA2.1-tubGal80(DE)-SV40*	*pAC-U63-gRNA2.1-tubBFP(HA)*	18	606025 & 606779
X	20F2	attP18	*pAC-U63-gRNA2.1-tubGal80(DE)-SV40*	*pAC-U63-gRNA2.1-tubBFP(HA)*	19	606026 & 606029
IV	101F1-a	attP[ZH-102D]**	*pAC-U63-gRNA2.1-tubGal80(DE)-SV40*	*pAC-U63-gRNA2.1-tubBFP(HA)*	4	606776 & 606780
IV	101F1-b	attP[ZH-102D]**	*pAC-U63-gRNA2.1-tubGal80(DE)-SV40*	*pAC-U63-gRNA2.1-tubBFP(HA)*	25	606777 & 606781
IV	101F1-c	attP[ZH-102D]**	*pAC-U63-gRNA2.1-tubGal80(DE)-SV40*	*pAC-U63-gRNA2.1-tubBFP(HA)*	28	606778 & 606782

Clone frequencies are measured by averaging clone numbers in 10 laterally mounted 3rd instar larvae with pMAGIC gRNA-markers. Only clones in A1 to A7 segments of one side of each larva were counted.
*Previously published gRNA-markers.
**3xP3-RFP has been removed from these lines.
***Detailed information for each line is available at https://bdsc.indiana.edu/stocks/misc/magic.html.

753